Spatial control of far-field structural sound radiation using structural sensors for broadband applications

Halim, D. and Cazzolato, B.S.

School of Mechanical Engineering, the University of Adelaide, SA 5005 Australia

ABSTRACT

The focus of the paper is to control the far-field sound radiation from an arbitrary planar structure using multiple structural sensors, particularly for broadband applications. A number of structural velocity sensors are distributed over the structure for sensing the sound radiation at a particular far-field region for control purposes. Spatial control of structural sound radiation is achieved by constructing a frequency-independent spatial filter that reflects the spatially-weighted sound radiation energy. Thus, the signal produced by the spatial filter can be used as an error signal to be minimised by standard active control methods. A numerical case study on the sound radiation of a flat panel structure is performed to investigate the control performance using the developed frequency-independent spatial filter.

INTRODUCTION

Research in structural sound radiation control has been intensive as reflected by the number of publications in this field, such as (Dimitriadis and Fuller 1992; Clark and Fuller 1991; Burgan et al. 2002). In many practical applications, it is important to be able to control the sound radiation to a particular far-field region, without wasting the control effort in attempting to control the entire far-field region. The work in this paper considers the active control of structural sound radiation with a spatially-weighted objective function that reflects the sound radiation energy at a particular far-field region. In this work, multiple structural sensors are used together with a spatial interpolation function to estimate the sound radiation in the far-field. The effectiveness of multiple structural sensors for vibration or sound radiation control has been demonstrated in various works such as in (Burgan et al. 2002; Meirovitch and Baruh 1982; Pajunen et al. 1994). The primary interest of this work is to consider a practical method which can be used to deal with the spatial control of sound radiation with broadband excitation.

SOUND RADIATION ESTIMATION

The active control strategy in this work requires the estimation of the far-field sound pressure radiated from a vibrating arbitrary structure. For this purpose, it is important to be able to estimate the vibration profile of the structure first.

Sensing the structural vibration

The approach used to estimate the vibration profile of a structure depends on the use of multiple structural sensors distributed over the structure. The advantage of this sensing approach is that it can be combined with a spatial interpolation function to estimate the vibration profile of the entire structure, not just at the locations of the sensors. In addition, the method does not require the a-priori information about the system's dynamic since all the vibration information required directly comes from the structural sensors.

The approach here follows the method proposed in (Halim and Cazzolato 2005). Consider an arbitrary structure in Figure 1 where N structural velocity sensors are used at a number of structural locations. In addition, N_o nodes at the structural boundaries where the vibration level is minimal are also used for the vibration estimation process. A number of nodes can be used to construct an element as shown in Figure 1 using a simple rectangular element, although other geometry can also be utilised.

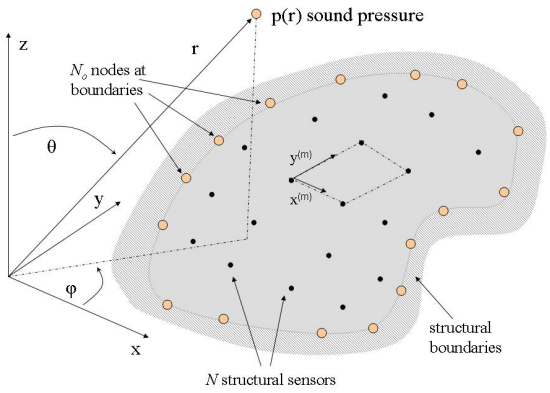

Figure 1 An arbitrary panel structure with N structural sensor nodes and N_o nodes at the structural boundaries. An element is constructed from several nodes and a spatial interpolation function is used to estimate the normal surface velocity to estimate the far-field sound radiation.

Suppose each m^{th} element (of M total number of elements) has local coordinates $(x^{(m)},y^{(m)})$. A transformation matrix $\boldsymbol{A}^{(m)}$ is used to transform the local coordinates to the global coordinates (x,y) shown in Figure 1. Therefore, the normal surface velocity $v(x,y)$ along the structure can be obtained from the normal velocity measurements from N structural sensors, $\boldsymbol{w}$ (Halim and Cazzolato 2005):

$$v(x,y) = \boldsymbol{H}(x^{(m)},y^{(m)})\boldsymbol{A}^{(m)}\boldsymbol{w} \tag{1}$$

where $\boldsymbol{H}(x^{(m)},y^{(m)})$ is a spatial interpolation matrix.

Sensing the far-field sound radiation

The estimated velocity profile of the structure can now be used to estimate the far-field sound radiation based on the Rayleigh integral (Wallace 1972; Fuller et al. 1996) assuming an infinite baffle configuration. The far-field complex sound pressure p at a distance r can be shown in terms of spherical coordinates shown in Figure 1:

$$p(\omega,r,\theta,\varphi) = \frac{j\omega\rho}{2\pi r}\int_R f(\omega,r,\theta,\varphi,x,y)v(x,y)dR \qquad (2)$$
$$f = \exp\{-jk(r - x\sin\theta\cos\varphi - y\sin\theta\sin\varphi)\}$$

Where ω is the frequency, R is the region of the structure, ρ is the density of the acoustic medium, and k is the acoustic wave number.

Since the normal surface velocity $v(x,y)$ can be estimated from Eq. (1), the far-field sound pressure can be estimated by considering the contributions of all M elements (Halim and Cazzolato 2005b):

$$\begin{aligned} p(\omega,r,\theta,\varphi) &= \kappa\exp(-jkr)\left\{\sum_{m=1}^{M} b^{(m)}\boldsymbol{P}^{(m)}\boldsymbol{A}^{(m)}\right\}\boldsymbol{w} \\ &= \kappa\boldsymbol{C}_p(\omega,r,\theta,\varphi)\boldsymbol{w} \end{aligned} \qquad (3)$$

where $\boldsymbol{C}_p$ can be found from the above expression and

$$\begin{aligned} &\kappa = \frac{j\omega\rho}{2\pi r} \\ &b^{(m)} = \exp\left(j\left(\alpha x_o^{(m)} + \beta y_o^{(m)}\right)\right) \\ &\boldsymbol{P}^{(m)} = \int_{y^{(m)}}\int_{x^{(m)}} \boldsymbol{H}\left(x^{(m)},y^{(m)}\right)\exp\left(j\left(\alpha x^{(m)} + \beta y^{(m)}\right)\right)dx^{(m)}dy^{(m)}. \\ &\alpha = k\sin\theta\cos\varphi \\ &\beta = k\sin\theta\sin\varphi \end{aligned} \qquad (4)$$

Here, $(x_o^{(m)}, y_o^{(m)})$ is the location of the m^{th} element's origin. Note that the sound pressure depends on the excitation frequency of the structure.

BROADBAND SPATIAL SOUND RADIATION CONTROL

It is now our interest to use the estimated far-field sound radiation pressure for constructing the objective function used for control purposes. Consider a fixed far-field radius at $r=r_o$. An objective function J that considers spatially weighted sound radiation energy can be described by (Halim and Cazzolato 2005b):

$$J(\omega) = \int_0^{2\pi}\int_0^{\pi/2} p(\omega,r_o,\theta,\varphi)^H q(\theta,\varphi)p(\omega,r_o,\theta,\varphi)d\theta d\varphi \qquad (5)$$

where $\{\}^H$ is the Hermitian transpose of a matrix and $q(\theta,\varphi)$ is a continuous spatial weighting function used to emphasise the spatial far-field region that needs to be controlled.

A broadband objective function will now be considered in this work by expanding Eq. (5) as:

$$\begin{aligned} J(\omega) &= \boldsymbol{w}(\omega)^H\{\int_0^{2\pi}\int_0^{\pi/2}\boldsymbol{C}_p{}^H(\omega,r,\theta,\varphi)q(\theta,\varphi) \\ &\quad\times\boldsymbol{C}_p(\omega,r,\theta,\varphi)d\theta d\varphi\}\boldsymbol{w}(\omega) \\ &\approx (j\omega\boldsymbol{w}(\omega))^H\{\left(\frac{\rho}{2\pi r}\right)^2\times\int_0^{2\pi}\int_0^{\pi/2}\boldsymbol{C}_p{}^H(\omega_c,r,\theta,\varphi) \\ &\quad\times q(\theta,\varphi)\boldsymbol{C}_p(\omega_c,r,\theta,\varphi)d\theta d\varphi\}(j\omega\boldsymbol{w}(\omega)) \end{aligned} \qquad (6)$$

where the objective function is approximated by evaluating the matrix $\boldsymbol{C}_p$ at a fixed frequency ω_c, chosen to be:

$$\omega_c = \frac{\omega_a + \omega_b}{2} \qquad (7)$$

Here, ω_a and ω_b can be taken respectively as the natural frequencies of the lowest and highest vibration modes within the frequency bandwidth of interest. The effectiveness of this objective function estimate for spatially controlling the sound radiation at different frequencies will be demonstrated in the following numerical study on a rectangular panel structure. It can also be note that the term $j\omega\boldsymbol{w}$ is the acceleration signal measured by the structural sensors so naturally accelerometers can be used to obtain this information.

The objective function can now be written as:

$$\begin{aligned} J(\omega) &\approx (j\omega\boldsymbol{w}(\omega))^H(\boldsymbol{G}+\beta\boldsymbol{I})(j\omega\boldsymbol{w}(\omega)) \\ &\approx (j\omega\boldsymbol{w}(\omega))^H\boldsymbol{U}\boldsymbol{V}\boldsymbol{U}^T(j\omega\boldsymbol{w}(\omega)) \\ &\approx (j\omega\boldsymbol{w}(\omega))^H\boldsymbol{\Gamma}^T\boldsymbol{\Gamma}(j\omega\boldsymbol{w}(\omega)) \\ &\approx \boldsymbol{z}(\omega)^H\boldsymbol{z}(\omega) \end{aligned} \qquad (8)$$

where $\boldsymbol{G}$ is obtained from the term inside the curved brackets in Eq. (6) that can be obtained using a numerical integration with respect to θ and φ coordinates. Furthermore, β and $\boldsymbol{I}$ are respectively a scalar small positive number and an identity matrix with compatible dimensions. The purpose of adding term $\beta\boldsymbol{I}$ is to ensure the positive definiteness of the matrix ($\boldsymbol{G}+\beta\boldsymbol{I}$) since small negative eigenvalues might occur when the integral is numerically calculated. The term β can be chosen appropriately to ensure that the characteristics of the dominant eigenvalues of $\boldsymbol{G}$ are not lost. Note that $\boldsymbol{U}$ and $\boldsymbol{V}$ are the matrices containing the eigenvectors and eigenvalues of ($\boldsymbol{G}+\beta\boldsymbol{I}$) respectively. In this case, $\boldsymbol{U}$ and $\boldsymbol{V}$ are different from the radiation modes approach proposed by Elliot and Johnson (1993) since the derivation here has taken into account the estimated vibration profile over the entire structure, as well as the continuous spatial weighting function $q(\theta,\varphi)$ for sound radiation in the far-field. Note that Elliot and Johnson (1993) utilise the elemental radiators approach for control of the overall acoustic sound radiation power.

The transformed signal $\boldsymbol{z}(\omega) = \boldsymbol{\Gamma}(j\omega\boldsymbol{w}(\omega))$ is essentially a signal that represents the spatially weighted sound radiation energy. The energy of this signal can be minimised using a standard active control method, so that consequently the objective function can also be minimised. It is important to observe that the spatial filter $\boldsymbol{\Gamma}$ is frequency-independent so that a simple filter implementation can be implemented for broadband spatial control.

NUMERICAL ANALYSIS OF RADIATED SOUND CONTROL

In this section, the effectiveness of the proposed method to control sound radiation for broadband applications will be investigated through a numerical study. For tonal cases, it is easier to see the performance of the developed spatial control strategy since the sound radiation profile in the far-field can be readily compared between the un-controlled and controlled cases. Thus, in this numerical study, different tonal control cases using a similar spatial filter are investigated. Satisfactory performances for different tonal cases would imply that the developed frequency-independent spatial filter can provide a good estimation of the spatially-weighted sound radiation energy within a frequency range that would be useful for broadband control applications.

Consider an aluminium simply-supported panel structure with 5x5 structural velocity sensors distributed over the panel. These 25 sensors would provide a reasonably accurate vibration profile estimation for vibration modes with m or n<4, which consists of the first 6 modes up to a frequency of approximately 533 Hz. The dimensions of the panel are 0.450m x 0.300mm x 0.0025m and the natural frequencies of the first 7 vibration modes are shown in Table 1. For estimating the vibration profile of the panel, a linear interpolation function is used (see Halim and Cazzolato 2005b). Point sources are used as disturbance and control sources and Figure 2 shows the locations of sensors, disturbance and control sources.

Table 1.The first 7 natural frequencies of the panel.

Mode	Frequency [Hz]
(1,1)	96.2
(2,1)	185.0
(1,2)	296.1
(3,1)	333.1
(2,2)	384.9
(3,2)	532.9
(4,1)	540.3

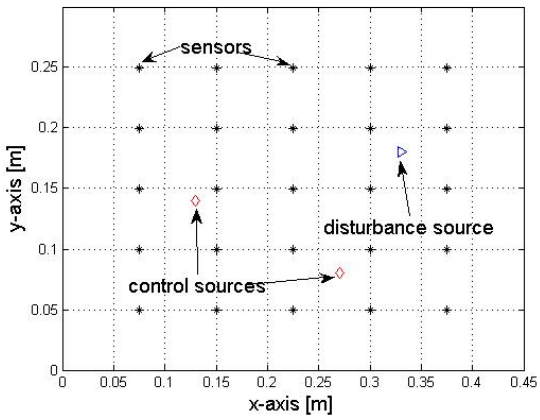

Figure 2 Locations of the sensors, disturbance and control sources used in the numerical study.

The eigenvalues of ($\boldsymbol{G}+\beta\boldsymbol{I}$) are plotted in Figure 3, where β=6.5x10^{-6} has been chosen to ensure the positive definiteness of the matrix. It can be shown that only a few dominant eigenvalues so it is decided that the contributions of the first 5 largest eigenvalues are used to compute matrix $\boldsymbol{\Gamma}$, so that only 5 error signals would be generated as the outputs of spatial filter $\boldsymbol{\Gamma}$. A continuous spatial weighting can now be used to emphasise the far-field region whose sound radiation energy needs to be minimised. Figure 4 shows the normalised spatial weighting function, where as Figure 5 illustrates the hemisphere far-field region in which the sound radiation control is of interest.

Using the obtained matrix $\boldsymbol{\Gamma}$, spatial control of sound radiation will be done for cases with varying excitation frequencies in order to investigate if the proposed spatial filter can be effective for spatial control. For this numerical study, a frequency bandwidth, containing the first 5 vibration modes, up to a frequency of about 390 Hz is considered. Thus, ω_c is calculated to be a middle frequency between natural frequencies of the first mode (96.2 Hz) and fifth mode (384.9 Hz). In order to easily visually the effect of the implemented spatial control on the far-field sound radiation profile, optimal tonal control at several excitation frequencies is considered in this study at a far-field radius of r=8 m.

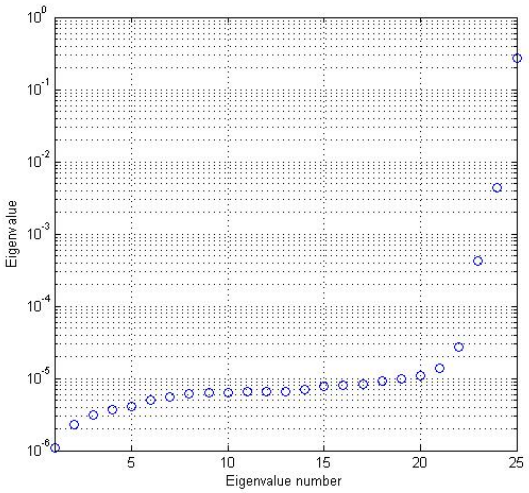

Figure 3 Eigenvalue plot of ($\boldsymbol{G}+\beta\boldsymbol{I}$), where the five largest eigenvalues are used for control purposes.

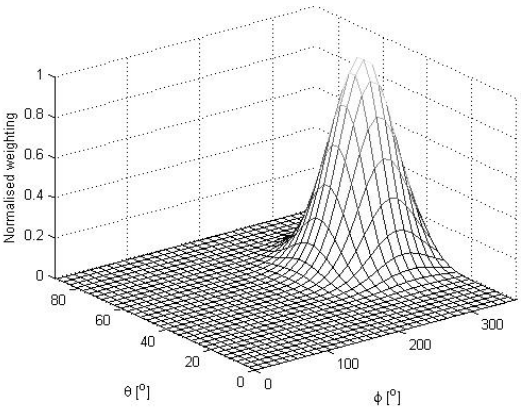

Figure 4 The normalised spatial weighting used for spatial control of sound radiation.

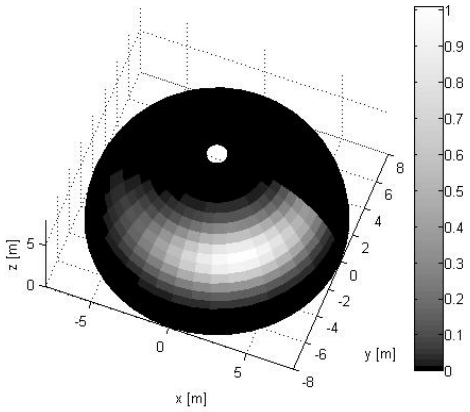

Figure 5 The far-field region emphasised by the spatial weighting function.

Sound radiation control at 100 Hz

The first numerical study considers a particular sound radiation control at 100 Hz which is close to the natural frequency of mode (1,1). As expected the far-field sound radiation profile of the un-controlled panel almost resembles a monopole-type sound radiation as illustrated in Figure 6. The gray colour variations in Figures 6 and 7 indicate the magnitude variation of the far-field radiation profiles. In particular, Figure 6 shows that there exists a small variation of sound radiation across the far-field region, although the monopole-type radiation still dominates. Figure 7 shows the change in the far-field sound radiation profile as an active control based on minimising the error signal generated by the spatial filter $\boldsymbol{\Gamma}$. Comparing the result with the spatial weighting function in Figure 4, it can be seen that the spatial control manages to reduces the region of higher weighting more than other regions. It also should be noted that the sound pressure level of the entire far-field region is also being reduced although the region with higher weighting experiences a better level of sound reduction.

The directivity plots with respect to x and y coordinates can be seen in Figures 8 and 9 respectively. The figures show the effect of spatial control in reducing the sound radiation where the dashed line and the solid line represent the results without control and with control respectively.

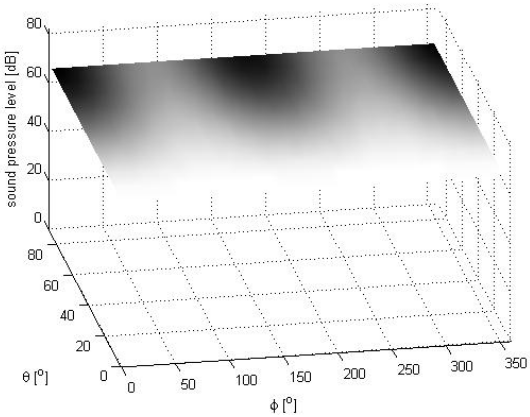

Figure 6 Far-field sound radiation profile of the panel at 100 Hz, without control.

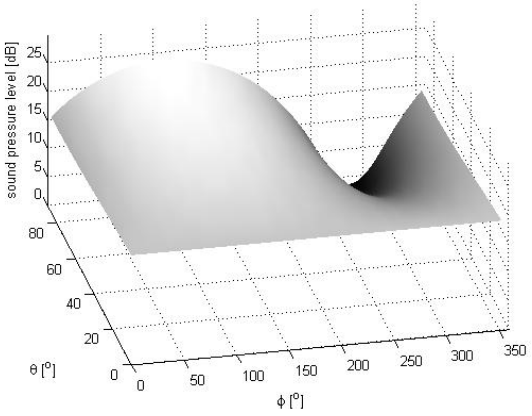

Figure 7 Far-field sound radiation profile of the panel at 100 Hz, with control.

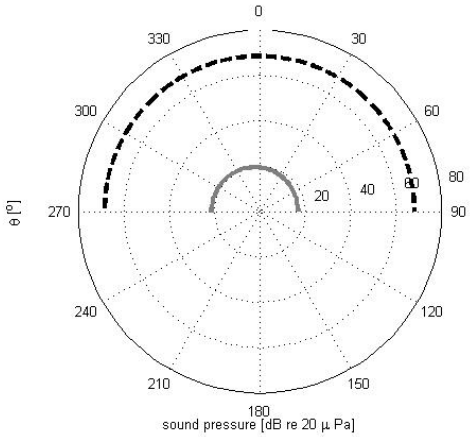

Figure 8 Directivity plots with respect to x-axis at 100Hz. Solid line: without control. Dashed line: with control.

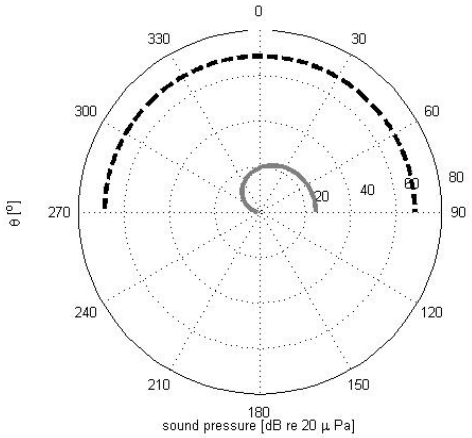

Figure 9 Directivity plots with respect to y-axis at 100 Hz. Solid line: without control. Dashed line: with control.

Sound radiation control at 340 Hz

The second study concentrates on attempting to control the sound radiation at a frequency of 340 Hz, which is close to the natural frequency of the 4th mode (3,1). The directivity plots with respect to x and y axes are shown in Figures 10 and 11 respectively. It is interesting to compare these results with the spatial weighting function shown on the far-field hemisphere in Figure 5. By considering the spatial weighting in the directions of x and y axes (i.e. taking the slices along x and y directions), it can be observed that the regions of high spatial weighting are the ones that received most sound reductions as shown in Figures 10 and 11 as expected.

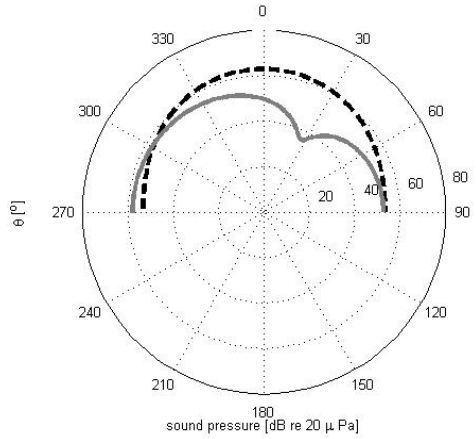

Figure 10 Directivity plots with respect to *x*-axis at 340 Hz. Solid line: without control. Dashed line: with control.

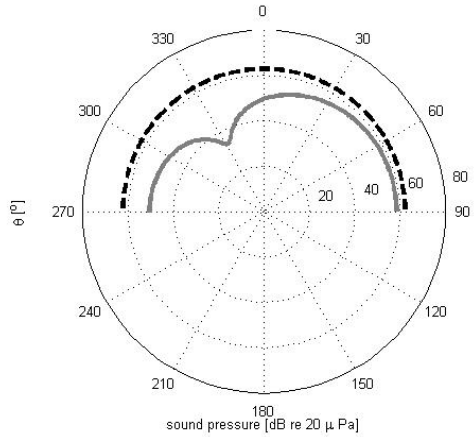

Figure 11 Directivity plots with respect to *y*-axis at 340 Hz. Solid line: without control. Dashed line: with control.

Sound radiation control at 380 Hz

The final study considers the frequency of 380 Hz, which is close to the natural frequency of the 5th mode (2,2). The results for the far-field sound radiation profile are shown in Figures 12 and 13. Again, the controller attempts to minimise the far-field region with high spatial weighting, which is reflected in the error signal that is obtained from the filtering of the acceleration signals with matrix $\boldsymbol{\Gamma}$. The directivity plots with respect to *x* and *y* axes are shown in Figures 14 and 15 respectively. It is interesting to note that from Figure 14, there are some regions whose sound radiation is actually being increased. The increase in sound radiation at some far-field regions can be expected as the control objective is only to minimise a partial region in the far-field, and not the entire region. However, Figure 15 also shows that the sound radiation is being reduced at the far-field region of interest. Obviously, the results from the directivity plots only consider the sound radiation profile along the *x* and *y* directions, so a more complete picture of the control performance should be observed from Figures 12 and 13 which shows the expected sound radiation reduction in the region with high spatial weighting.

Considering the control performances for the 3 different excitation frequencies within the bandwidth of interest, it can be observed that the sound radiation reduction was achieved in the region with high spatial weighting as expected. The frequency-independent spatial filter $\boldsymbol{\Gamma}$ computed using the proposed method has been used for all 3 control cases, which demonstrates that the developed spatial filter can be effectively used for broadband spatial sound radiation control applications.

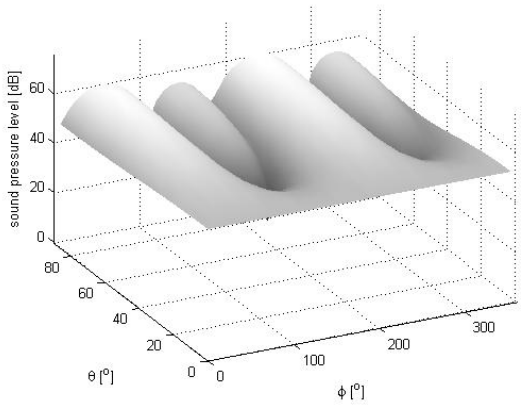

Figure 12 Far-field sound radiation profile of the panel at 380 Hz, without control.

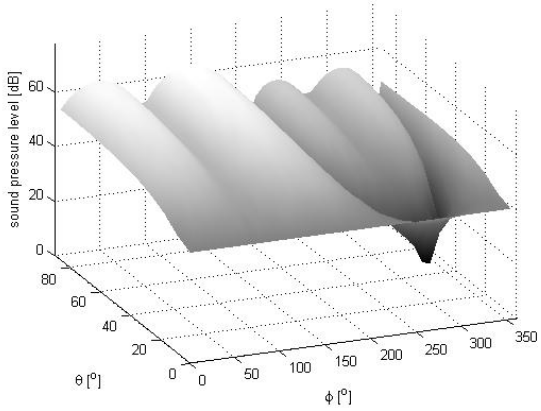

Figure 13 Far-field sound radiation profile of the panel at 380 Hz, with control.

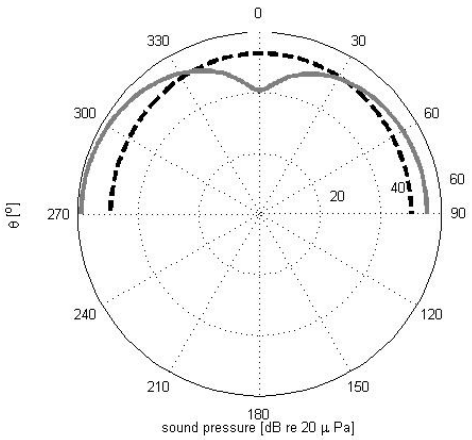

Figure 14 Directivity plots with respect to *x*-axis at 380 Hz. Solid line: without control. Dashed line: with control.

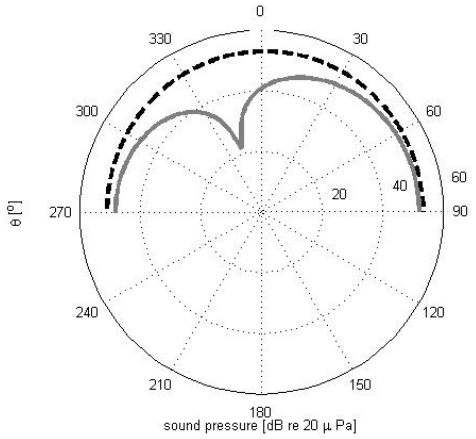

Figure 15 Directivity plots with respect to ***y***-axis at 380 Hz. Solid line: without control. Dashed line: with control.

CONCLUSIONS

The proposed method for controlling the structural sound radiation at a spatial far-field region for broadband applications has been presented. A frequency-independent spatial filter is utilised to obtain an error signal, representing the spatial sound radiation energy that can be minimised by standard control methods. Numerical studies on a rectangular panel showed that its spatial sound radiation can be controlled even when the excitation frequency is varied within the frequency bandwidth of interest, indicating a satisfactory performance of the developed spatial filter to be used for broadband control applications.

ACKNOWLEDGEMENTS

Support from the Australian Research Council is gratefully acknowledged by the authors.

REFERENCES

Burgan, NC, Snyder, SD, Tanaka, N and Zander, AZ 2002, "A generalised approach to modal filtering for active noise control – Part I: Vibration sensing", *IEEE Sensors Journal*, vol. 29, no. 6, pp. 577-589.

Clark, RL and Fuller, CR 1991, "Control of sound radiation with adaptive structures", *Journal of Intelligent Material Systems and Structures*, vol. 2, p. 431-452.

Dimitriadis, EK and Fuller, CR 1992, "Active control of sound transmission through elastic plates using piezoelectric actuators", *American Institute of Aeronautics and Astronautics Journal*, vol. 29, no. 11, pp. 1771-1777.

Elliot, SJ 2001, *Signal processing for active control*, Academic Press, London.

Elliot, SJ and Johnson, ME 1993 "Radiation modes and the active control of sound power", *Journal of Acoustical Society of America,* vol. 94, no. 4, pp.2194-2204.

Fuller, CR, Elliot, SJ and Nelson, PA 1996, *Active control of vibration*. Academic Press, London.

Halim, D and Cazzolato, BS 2006, "A multiple-sensor method for control of structural vibration with spatial objectives", *Journal of Sound and Vibration*, vol. 296, pp. 226-242.

Halim, D and Cazzolato, BS 2005b, "Active control of structural sound radiation using a spatial control method with multiple structural sensors", *Proc. 44th IEEE Conference on Decision & Control and European Control Conference 2005*, Spain.

Meirovitch, L and Baruh, H 1982, "Control of self-adjoint distributed parameter systems", *Journal of Guidance*, vol. 5, no. 1, pp. 60-66.

Pajunen, GA, Neelakanta, PS, Gopinathan, M and Arockaisamy, M 1994, "Distributed adaptive control of flexible structures", *SPIE Proc. 1994 North American Conference on Smart Structures and Intelligent Systems*, pp.2190:790-801.

Wallace, CE 1972, "Radiation resistance of a rectangular panel", *Journal of the Acoustical Society of America*, vol. 51, pp. 946-952.